On the Influence of Pitching and Acceleration on Vortex Dynamics Around Low-Aspect-Ratio Rectangular Wings

Ryan Jantzen* and Kunihiko Taira†
Florida State University, Tallahassee, FL
Kenneth Granlund‡ and Michael V. Ol§
U.S. Air Force Research Laboratory, Wright-Patterson Air Force Base, OH

In the present study, we use numerical simulations to investigate the three-dimensional flows over low-aspect-ratio flat plates undergoing two canonical motions at low Reynolds numbers. The first motion is defined by the flat plate initially translating at 0° incidence that pitches to 45° about its leading edge. The second motion consists of the flat plate at a constant 45° incidence in a quiescent fluid, where the plate accelerates up to a constant velocity. The focus of this study is to investigate the influence of these simplified motions on the unsteady vortex dynamics, specifically the formation and evolution of the leading-edge, trailing-edge, and tip vortices over the low-aspect-ratio plate. A parameter study of Reynolds number, aspect ratio and pitch rate is performed to further understand the effect of these motions on the complex flow field.

I. Introduction

As we pursue improvement of aircraft maneuverability, the aircraft is expected to have predictable high aerodynamic performance at high angles of attack and to operate in gusty conditions. While this is necessary for large-size conventional aircraft, it is also critical for unmanned air vehicles that are designed to fly in urban environment where wake generated behind buildings and atmospheric fluctuations pose a challenge to stable flight operations. In order to achieve desirable flight performance at these conditions, it becomes necessary to develop an accurate aerodynamic force model for unsteady wing motions with large amplitudes. Compared to past quasi-steady type force theories, it is critical to account for the massively separated regions that form behind wings and the influence of large-scale three-dimensional vortices. In the proposed investigation, we will focus on highlighting the vortex dynamics of the wake behind wings undergoing large-amplitude canonical motion. The understudying from the vortex formation and evolution will allow for better prediction of lift and drag forces on aircraft that pursues such agile motions.

There have been numerous experimental and numerical studies for the unsteady aerodynamics associated with the complex motions of UAV/MAV flight for three-dimensional flat plates. Taira and Colonius[1] used simulations to explore the three-dimensional behavior of the flow over low-aspect-ratio flat plates. They observed that the tip vortices due to the three-dimensionality of the low-aspect-ratio plate help stabilize the flow for impulsively started flows. Granlund et al.[2] examined the three-dimensional vortex structure using dye-visualization and direct force measurements for rectangular and Zimmerman planforms undergoing high-frequency, high-amplitude linear pitch ramps. In the study by Chen, Colonius, and Taira,[3] they have examined the influence of acceleration on short and long time behavior of the wake and aerodynamic forces on a two-dimensional flat-plate wing at high angle of attack. Garmann and Visbal[4] computed the effect of acceleration and Reynolds number for high-amplitude pitch-ramp motions, revealing that the unsteady

*Graduate Research Assistant, Department of Mechanical Engineering, rtj09@my.fsu.edu.
†Assistant Professor, Department of Mechanical Engineering, ktaira@fsu.edu.
‡Post-Doctoral Scholar, Air Vehicles Directorate, Kenneth.Granlund.ctr@wpafb.af.mil
§Senior Aerospace Engineer, Air Vehicles Directorate, Michael.Ol@wpafb.af.mil.

Report Documentation Page

Form Approved
OMB No. 0704-0188

1. REPORT DATE	2. REPORT TYPE	3. DATES COVERED
JAN 2013		**00-00-2013 to 00-00-2013**

4. TITLE AND SUBTITLE	5a. CONTRACT NUMBER
On the Influence of Pitching and Acceleration on Vortex Dynamics Around Low-Aspect-Ratio Rectangular Wings	5b. GRANT NUMBER
	5c. PROGRAM ELEMENT NUMBER
6. AUTHOR(S)	5d. PROJECT NUMBER
	5e. TASK NUMBER
	5f. WORK UNIT NUMBER
7. PERFORMING ORGANIZATION NAME(S) AND ADDRESS(ES) **Air Force Research Laboratory,Air Vehicles Directorate,Wright Patterson AFB,OH,45433**	8. PERFORMING ORGANIZATION REPORT NUMBER
9. SPONSORING/MONITORING AGENCY NAME(S) AND ADDRESS(ES)	10. SPONSOR/MONITOR'S ACRONYM(S)
	11. SPONSOR/MONITOR'S REPORT NUMBER(S)

12. DISTRIBUTION/AVAILABILITY STATEMENT
Approved for public release; distribution unlimited

13. SUPPLEMENTARY NOTES
51st AIAA Aerospace Sciences Meeting and Exhibit, Grapevine, TX, 7-10 Jan 2013.

14. ABSTRACT

15. SUBJECT TERMS

16. SECURITY CLASSIFICATION OF:			17. LIMITATION OF ABSTRACT	18. NUMBER OF PAGES	19a. NAME OF RESPONSIBLE PERSON
a. REPORT **unclassified**	b. ABSTRACT **unclassified**	c. THIS PAGE **unclassified**	**Same as Report (SAR)**	**12**	

aerodynamic loads are insensitive to acceleration of the plate and that the aerodynamic loads compare closely with the same motions at lower Reynolds numbers. Yilmaz and Rockwell[5] used qualitative visualization to investigate the onset and evolution of the three-dimensional flow structures for rectangular and elliptical low-aspect-ratio flat plates for a pitch up maneuver. Calderon et al.[6] compared volumetric velocimetry measurements with computational results for low aspect ratio wings subjected to small amplitude pure plunging motion. They found that the three-dimensional leading edge vortex is highly dependent on the frequency at which the motion takes place. To highlight the influence of vortical forces, Lee et al.[7] quantified the contributions of vorticity to the forces exerted on a finite-aspect-ration flat plate using the vorticity force analysis (VFA). They noted that the interplay between the leading-edge vortex and tip vortices play a key role in distinguishing the force contributions for a plate with a smaller aspect ratio than that with a larger one.

In the present study, we investigate the three-dimensional flow structure and resulting forces on a low-aspect-ratio rectangular flat plate undergoing two different motion profiles at Reynolds numbers of 14 to 500. The first motion is defined by a flat plate initially translating at 0° incidence that pitches about its leading edge to 45°. The second motion consists of a flat plate initially at an angle of attack of 45° in a quiescent fluid in which it then accelerates up to a constant velocity. We will perform a parameter study with varied aspect ratio ($AR = 1, 2$, and 4), and Reynolds number ($Re = 14$ to 500) at a reduced frequency of $k = \pi/8$ and $\pi/48$ for both the pitching and accelerating motions to try to further understand the effect these parameters have on the vortical structures and unsteady aerodynamic forces on the wing. The motion frequency for both the pitching and acceleration motions have been defined by the NATO AVT-202 Task Group as the number of chords traveled during acceleration. The cases that are pursued in the present study include motions to take place over 1 chord length of travel (fast case) and 6 chord lengths of travel (slow case). The overall objective in the current study is to investigate the influence of pitching and acceleration on the vortex dynamics of three-dimensional wake vortices behind the low-aspect-ratio wing in laminar flow. The unsteady aerodynamics force results from numerical simulations are compared to force measurements from water-tunnel experiments performed at the Air Force Research Laboratory (Wright-Patterson). There is also a companion paper that focuses on the aerodynamic force exerted on the wings undergoing a wide variety of canonical motions.[8]

II. Numerical Simulation

A. Methodology

The three-dimensional incompressible flow over a low-aspect-ratio flat-plate wing is simulated with an immersed boundary projection method.[9] This method allows a body of arbitrary geometry to be generated on a Cartesian grid by adding appropriate boundary forces along the immersed boundary, represented by a set of Lagrangian points, to enforce the no-slip boundary condition. The continuous analog of the immersed boundary method can be given in the non-dimensional form by:

$$\frac{\partial \mathbf{u}}{\partial t} + \mathbf{u} \cdot \nabla \mathbf{u} = -\nabla p + \frac{1}{Re} \nabla^2 \mathbf{u} + \int_s \mathbf{f}\left(\boldsymbol{\xi}(s,t)\right) \delta\left(\boldsymbol{\xi}(s,t) - \mathbf{x}\right) ds, \tag{1}$$

$$\nabla \cdot \mathbf{u} = 0, \tag{2}$$

$$\mathbf{u}\left(\boldsymbol{\xi}\left(s,t\right)\right) = \int_{\mathbf{x}} \mathbf{u}\left(\mathbf{x}\right) \delta\left(\mathbf{x} - \boldsymbol{\xi}\right) d\mathbf{x} = \mathbf{u}_B\left(\boldsymbol{\xi}\left(s,t\right)\right), \tag{3}$$

$$\tag{4}$$

where $\mathbf{u}$, p and $\mathbf{f}$ are the non-dimensionalized velocity, pressure and surface force, respectively. The velocity, spatial coordinate, and pressure are normalized by the free stream velocity U_∞, chord length c, and ρU_∞^2 with ρ representing the density of fluid. The temporal variable is reported in terms of the non-dimensional convective time unit, normalized by c/U_∞. The spatial variables in the computational domain $\mathscr{D}$ and on the surface $\partial\mathscr{B}$ are denoted with $\mathbf{x}$ and $\boldsymbol{\xi}$, respectively. The Reynolds number is defined by $Re \equiv U_\infty c/\nu$, where ν is the kinematic viscosity of the fluid.

The immersed boundary projection method enforces both the incompressibility and no-slip constraints through a single projection in a manner similar to the projection used to satisfy incompressibility in the traditional fractional-step methods. The governing equations, Eq. (1) to (3), are spatially discretized us-

ing a second-order finite-volume formulation on a staggered grid. The convective and viscous terms are integrated in time with the second-order Adams–Bashforth and Crank–Nicolson schemes, respectively, to provide second-order accuracy in time. The boundary surface is represented by set of discrete delta functions to model infinitely thin flat-plate wings. The planform of the wing is set to be rectangular with an aspect ratio of 1, 2, and 4.

The computational domain consists of a large rectangular box of size of $[-4,6] \times [-5,5.7] \times [-6,6]$ in the streamwise, vertical, and spanwise directions. The midspan of the leading edge is positioned at the origin and the rectangular plate is set into a prescribed motion. The boundary conditions along all sides of the computational boundary $\partial\mathscr{D}$ are set to uniform flow $(U_\infty, 0, 0)$ except for the outlet boundary where a convective boundary condition $(\partial\mathbf{u}/\partial t + U_\infty \partial\mathbf{u}/\partial x = 0)$ is specified. The grid is stretched away from the wing to reduce the number of grid points required for the simulation.

The method has been validated for a variety of flows,[9] including separated flows around low-aspect-ratio wings in rectilinear motion.[1] Validation for the current pitching and accelerating motions are provided using force data from water-tunnel experiments performed at the Air Force Research Laboratory (Wright-Patterson). The forces on the flat plate (F_x, F_y, F_z) are given in terms of the non-dimensional lift, drag and side forces defined by $C_L = F_y/\left(\frac{1}{2}\rho U_\infty^2 A\right)$, $C_D = F_x/\left(\frac{1}{2}\rho U_\infty^2 A\right)$ and $C_S = F_z/\left(\frac{1}{2}\rho U_\infty^2 A\right)$, respectively, where A is the area of the flat plate. The freestream velocity will be either the steady-state or instantaneous value depending on the wing motion, which will be specified in the text.

III. Results

A. Pitching Maneuver

The first maneuver considered during the discussion of the present results is pitching about leading edge of the wing as shown in Figure 1. The simulation begins with the flat plate wing held stationary in a uniform free stream initially at a zero degree incidence. After sufficient time has passed for the initial transients of the simulation to decay, the wing begins its pitching maneuver. The angle of attack history is given by a linear ramp, corresponding to a constant angular acceleration. Due to the discontinuity in the derivatives at the beginning and end of the ramp function, which results in infinite spikes in the aerodynamic loading, we employ a modified version of the Eldredge function[10] to smooth out the discontinuities. The angle of attack history for this smoothed linear ramp is given by:

$$\alpha(\tau) = \frac{\Omega_\circ}{2a} \ln\left[\frac{\cosh\left(a\left(\tau - \tau_1\right)\right)}{\cosh\left(a\left(\tau - \tau_2\right)\right)}\right] + \frac{\alpha_{\max}}{2}, \tag{5}$$

where a is the smoothing parameter, $\Omega_\circ = \alpha_{\max}/t_{\text{pitch}}$ is the nominal non-dimensional pitch rate, and $t_{pitch} = \tau_1 - \tau_2$ is the pitching interval. For the present study, two different pitching intervals were considered, $t_{\text{pitch}} = 1$ corresponding to pitching over 1 chord length of travel (fast pitching) and $t_{\text{pitch}} = 6$ corresponding to pitching over 6 chord lengths of travel (slow pitching). The maximum angle of attack considered for all studies is $\alpha_{\max} = 45°$, which results in reduced frequencies of $k = \pi/8$ and $\pi/48$ for the fast and slow pitching cases, respectively.

Figure 1 illustrates the kinematics for the present pitching studies as well as the resulting coefficient of lift for an $AR = 2$ wing operating at $Re = 300$. The left axis represents the coefficient of lift, designated by the red curve, while the right axis represents the angle of attack history in degrees, designated by the blue curve. For the case considered here, $\tau_1 = 0$ and $\tau_2 = 1$, corresponding to $t_{\text{pitch}} = 1$ (fast pitching). We note that the convective time scale has is shifted for visual purposes to accommodate the beginning of the pitching maneuver to be centered around $\tau = 0$. The inserted snapshots in Figure 1 represents the vortical structure around the pitching wing during the maneuver. The three-dimensional vortex structures around the wing are given by the iso-surface of the Q-criterion ($Q = 3$), which for incompressible flows is given by $Q = \frac{1}{2}\left(\|\Omega\|^2 - \|S\|^2\right)$, where $\Omega = \frac{1}{2}[\nabla u - (\nabla u)^T]$ and $S = \frac{1}{2}[\nabla u + (\nabla u)^T]$ are the anti-symmetric and symmetric components of the velocity gradient tensor ∇u. Positive values of the Q-criterion, or Q-value, represent coherent structures which highlight regions of high swirl in comparison to shear.[11] The iso-surfaces colored by contours of constant pressure to identify regions of low pressure for the developing vortex structure. As the plate begins to pitch at $\tau = 0$, a large spike appears in the lift force due to the non-circulatory force from the initial angular acceleration. The amplitude of this non-circulatory peak is a direct function of the smoothing parameter a. Large values of a result in sharper transients, resulting in larger non-circulatory peak lifts, whereas small values of a result in smoothed transients, resulting in

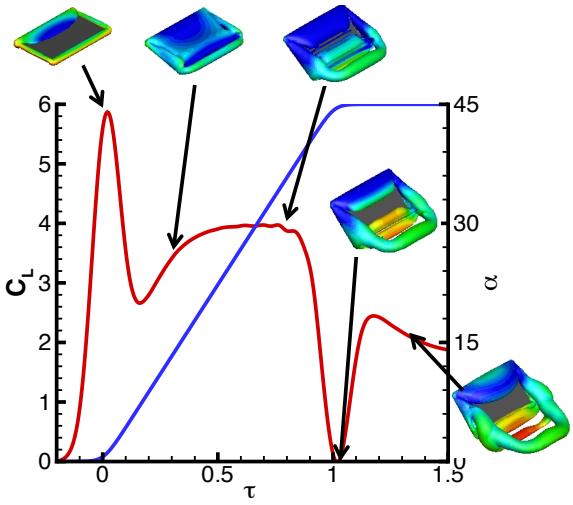

Figure 1. Coefficient of lift (red) and angle of attack history (blue) for an $AR = 2$ flat plate pitching over one chord length of travel at $Re = 300$. The three-dimensional vortical structure is visualized using a Q-value of $Q = 3$ and the isosurface is colored by contours of constant pressure.

lower non-circulatory peaks. As the plate continues to increase its angle of attack, the lift increases due to circulatory effects resulting from the low-pressure vortical structure forming over the top surface of the wing. In the following sections, we perform a parameter study of Reynolds number, aspect ratio, and pitch-rate to further understand the influence that pitching has on the vortex dynamics.

1. Reynolds number effect

We first consider the effect that Reynolds number has on the aerodynamic forces for the $AR = 4$ flat plate undergoing the pitching motion over one chord length of travel (fast pitching), given in Figure 2. Coefficients of lift and drag for $Re = 14, 25, 50, 100, 300$, and 500 from the present simulations (solid lines) are compared with force histories from water tunnel experiments at $Re = 10,000$ (dashed line). As previously mentioned, at the beginning of the pitching maneuver, the initial peak in the lift force is associated with the non-circulatory loading due to the initial angular acceleration of the plate. As the plate continues to increase its incidence with respect to the flow, the lift is once again increased to a second peak value. This is due to the low-pressure core of the leading-edge vortex forming over the suction side of the wing. We observe that as the Reynolds number is increased, the slope of the lift curve due to the circulatory effects increases and the point at which maximum circulatory lift is achieved occurs earlier in time. At the end of the pitching maneuver, the plate experiences a reduction in lift due to the angular deceleration of the plate, which is also a non-circulatory effect. After the pitching maneuver has completed, the lift begins to slowly decrease until it reaches a value of about 1.5 for all cases considered. We observe that for $Re > 100$, the history for both the lift and drag forces agree very well with the experimental force data. We believe that for these fast pitching motions, above a certain Re (around 100), the aerodynamic forces are mostly due to pressure dominant physics, whereas for Reynolds numbers below 100, the effect of viscous shear force dominates.

Next, we consider the three-dimensional flowfield over the flat-plate wing for $Re = 50, 100, 300$, and 500. Figure 3 shows the evolution of the three-dimensional flow field for these Reynolds numbers at various times. The Q-value used to visualize the current simulations is given by $Q = 0.5, 1, 3$, and 5 for $Re = 50, 100, 300$, and 500, respectively. We begin visualizing the flow field at $\tau = 0$, the point around which the pitching motion starts (note that $a > 0$ smears in initial pitching). Between $\tau = 0$ and $\tau = 1$, the wake vortices for different Re share the same topology. By $\tau = 1$ for each of the Reynolds numbers considered, counter-rotating tip vortices have formed at the tips of the wing due to the pressure difference between the top and bottom surfaces of the wing, the starting vortex has rolled up at trailing edge of the wing, and a leading-edge vortex begins to form over the top surface of the wing which is initially pinned at the corners of the leading edge. Thereafter, the trailing-edge vortex detaches and advects downstream in the form of a vortex ring while the leading-edge and tip vortices continue to roll up. As the wing continues to translate at its maximum angle

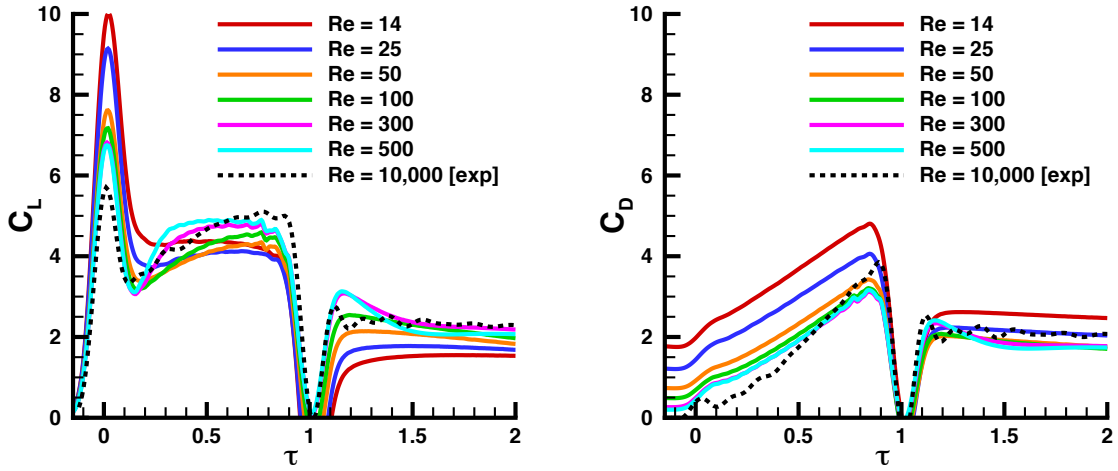

Figure 2. Reynolds number effect on the aerodynamic loading for $AR = 4$ wing pitching over one chord length of travel.

of attack, the developing leading-edge vortex detaches from the corners of the leading edge and resembles a hairpin vortex, which is also reported by Visbal[12] for pitching flat plates at $Re \approx 10^3 - 10^4$. We note that for the Reynolds numbers considered here, the vortex structures have similar features with respect to the leading edge, trailing edge and tip vortices. A major difference is observed as the Reynolds number is increased from $Re = 300$ to 500, where instabilities become present in the vortex structures. Although these instabilities are present in the flowfield, their effect is minimal on the aerodynamic forces generated on the wing. This is also observed by Garmann and Visbal[4] for pitching airfoils at much higher Reynolds numbers.

2. Aspect ratio effect

We now consider the effect on the aerodynamic forces that the aspect ratio plays for the pitching flat plate over one chord length of travel (fast pitching) operating at $Re = 300$, given in Figure 4. The aspect ratios considered for the present study include $AR = 1, 2$, and 4. We also plot the $AR = 2$ and 4 as well as the nominal 2-dimensional (wall to wall) forces from experiments. As the pitching motion begins, a non-circulatory spike is present due to the initial angular acceleration of the plate. As the aspect ratio is increased, the maximum value of this initial spike increases. Thereafter, lift is once again increased due to circulatory effects resulting from the vortex structure forming over the wing surface. As the aspect ratio is increased, the slope of the lift curve increases. We note that the lift reaches a plateau around $\tau = 0.3$ for the three aspect ratios considered. Once this plateau is reached for the $AR = 2$ and 4 wings, it remains at this value until the deceleration portion of the motion occurs, whereas it begins to slightly decrease for the $AR = 1$ case. Once the plate has reached its maximum angle of attack at $\tau = 1$, there is a negative spike in lift due to the angular deceleration of the plate. We note that in contrast to the minimal effect of due to the Reynolds number of the flow, the aspect ratio of the pitching wing plays a major contribution in the forces generated for the pitching maneuver.

Next, we consider the three-dimensional flowfield over the flat-plate wing for aspect ratios of $1, 2$, and 4, given in Figure 5. The vortical structure is visualized by an isosurface of $Q = 3$, colored in contours of constant pressure. We begin visualizing the flowfield at $\tau = 0$, the point around which the motion starts. We note that the vortex structure for the $AR = 1, 2$, and 4 wings look very similar early in time between $\tau = 0$ to $\tau = 1$, where the $AR = 2$ and 4 cases resemble stretched versions of the $AR = 1$ case. By $\tau = 1$ for the three aspect ratios considered, counter-rotating tip vortices have formed at the tips of the wing due to the pressure difference between the top and bottom surfaces of the wing, the starting vortex has rolled up at the trailing-edge of the wing, and a leading-edge vortex begins to form over the top surface of the wing which is initially pinned at the corners of the leading edge. Thereafter, the leading-edge vortex detaches from the wing for the $AR = 2$ and 4 plates, but stays attached for the $AR = 1$ case. This attachment is due to the presence of the counter-rotating tip vortices stabilizing the leading-edge vortex. As the wing

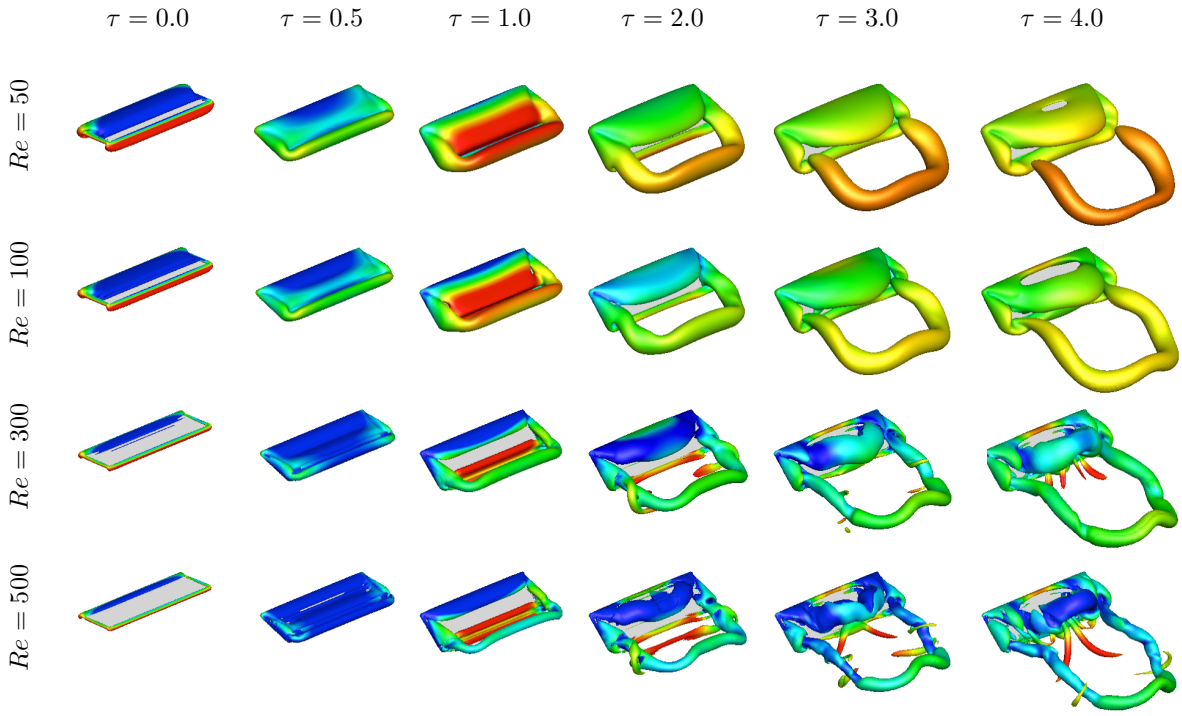

Figure 3. Flowfield images illustrating the Reynolds number effect for the $AR = 4$ wing pitching over one chord length of travel. The Q-value used to visualize the vortical structure is given by $Q = 0.5, 1, 3,$ and 5 for $Re = 50, 100, 300,$ and 500, respectively, and is colored in contours of constant pressure.

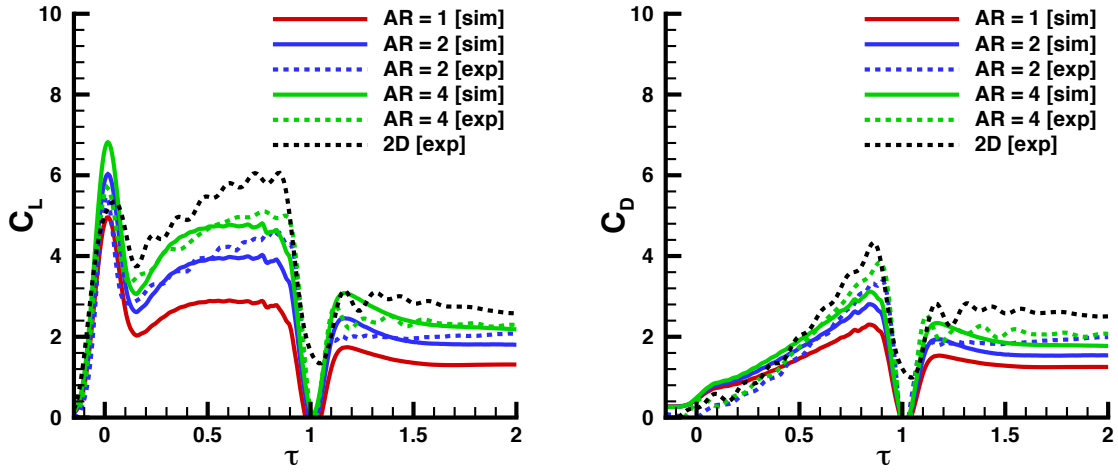

Figure 4. Aspect ratio effect on the aerodynamic loading for a wing pitching over one chord length of travel at $Re = 300$ (simulation; solid lines) and $Re = 10,000$ (experimental; dashed lines).

continues to translate at its maximum incidence of $\alpha = 45°$, the detached leading-edge vortex resembles a hairpin vortex, which advects down the top surface of the wing. We observe that this hairpin vortex remains near the top surface of the wing for the $AR = 2$ case compared to the $AR = 4$ case, which again is due to the counter-rotating tip vortices applying downward induced velocity onto the leading-edge vortex.

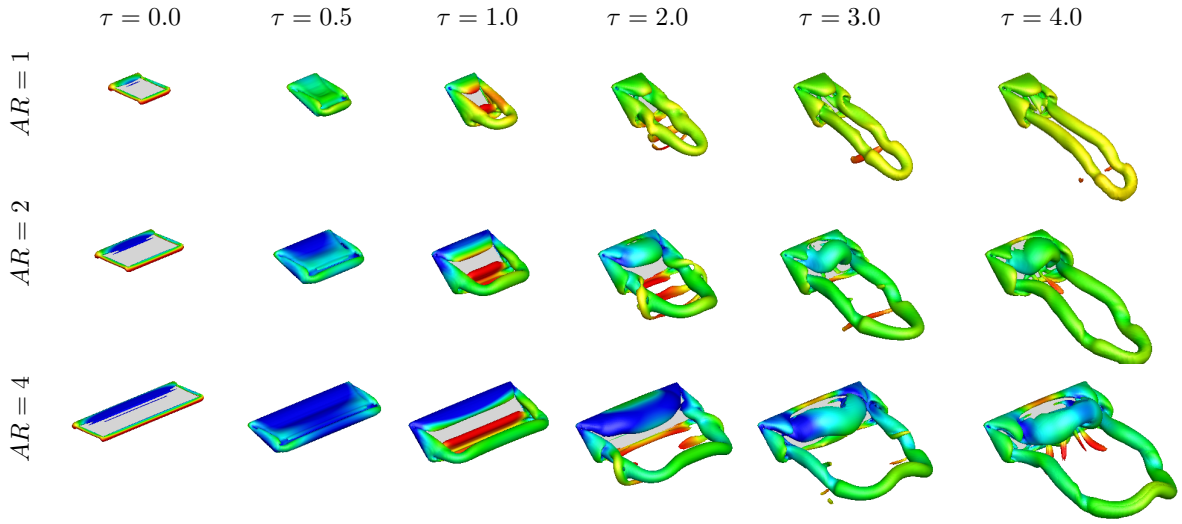

Figure 5. Flowfield images illustrating the effect of aspect ratio for a wing pitching over one chord length of travel at $Re = 300$. The vortical structure is visualized by an isosurface of $Q = 3$, colored in contours of constant pressure.

3. Pitch rate effect

We will now consider the effect that the frequency at which the motion takes place has on the aerodynamic forces for the $AR = 1, 2$ and 4 pitching plate at $Re = 300$. The pitching motion for the current case takes place over 6 chord lengths of travel ($k = \pi/48$). As seen in Figure 6, at the beginning of the motion ($\tau = 0$), we no longer observe the non-circulatory spikes that were present in the 1 chord length of travel cases due to the smoothing of the linear ramp profile for this reduced frequency. As the wing increases its angle of attack, we observe that the slope of the lift curve increases and and the peak lift value occurs earlier in time as the aspect ratio increases. For example, for the $AR = 4$ simulation case, the maximum lift occurs around $\tau = 4$ and then begins to decrease, resulting from dynamic stall. This observation is also present for the experimental data, except for the amplitude is greater and stall occurs later in time when compared to the simulation results. We note that this increased lift is attributed to the much larger Reynolds number ($Re = 10,000$), which results in greater circulatory effects. We also observe for the present case of pitching over 6 chord lengths of travel, the maximum lift achieved is much less than what was observed for the 1 chord length cases. Therefore, if an increase in lift is desired, these results show that larger reduced frequencies are required for a given Reynolds number and aspect ratio.

Figure 7 illustrates the three-dimensional flowfield over the flat-plate wing pitching over 6 chord lengths of travel at $Re = 300$ for $AR = 1, 2$, and 4. The vortical structure forming around the wing is visualized by an iso-surface of $Q = 3$, colored in contours of constant pressure. As the wing begins to increase its angle of attack, we observe that the formation of the leading-edge, trailing-edge, and tip vortices occurs much later in time for this motion compared to the 1 chord length pitching cases. By the end of the pitching maneuver ($\tau = 6$), the leading-edge vortex for the $AR = 2$ and 4 cases has detached from the corners of the leading-edge and forms a hairpin vortex which is similar to what is observed for the faster pitching cases for the $AR = 2$ and 4 wings. We also observe that for the present pitching cases over 6 chord lengths of travel, the value of the contours of constant pressure that the iso-surface of the Q-value is colored in is greater than what was observed for the 1 chord length cases. This reduced pressure attributes to the reduction in lift compared to the faster motion due to the lack of the low pressure cores of the leading-edge, trailing-edge and tip vortices over the top surface of the wing.

B. Accelerating Maneuver

The second motion we consider in this study is a linear acceleration of the wing from rest. Initially, the wing sits in a quiescent fluid at a fixed incidence of $\alpha = 45°$. The plate is then set into motion using the modified Eldredge function for the acceleration profile, which results in a linear acceleration from rest up to

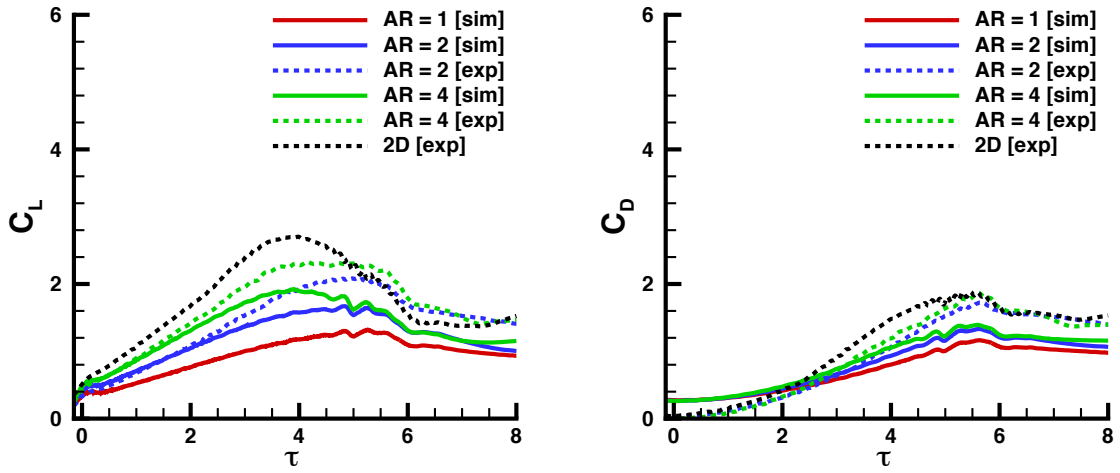

Figure 6. Aspect ratio effect on the aerodynamic loading for a wing pitching over six chord lengths of travel at $Re = 300$ (simulation; solid lines) and $Re = 10,000$ (experimental; dashed lines).

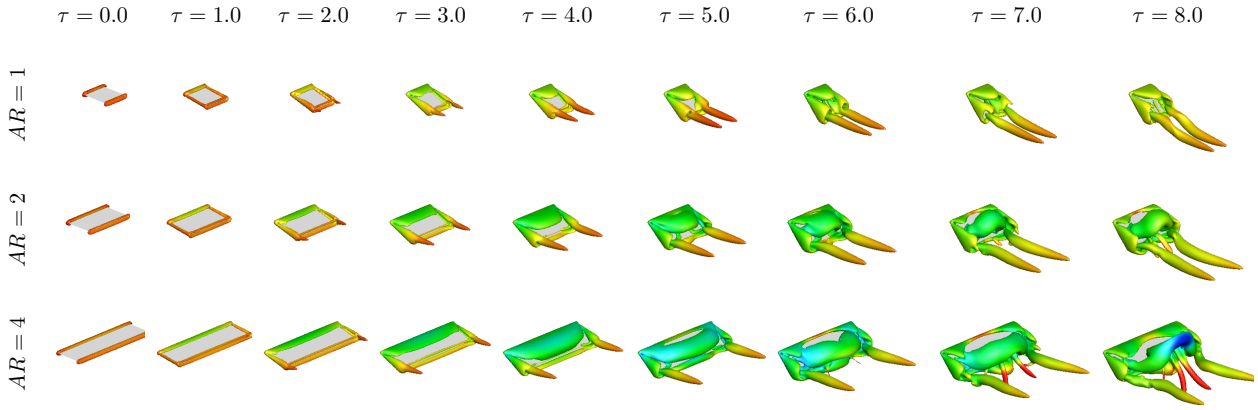

Figure 7. Flowfield images illustrating the effect of aspect ratio for a wing pitching over six chord lengths of travel at $Re = 300$. The wake vortices are visualized by an isosurface of $Q = 3$, colored by contours of constant pressure.

a maximum freestream velocity that corresponds to final instantaneous Reynolds number. For the current study, the accelerated motion occurs over 1 chord length and 6 chord lengths of travel. We focus on very low Reynolds number flows of $Re = 14, 25, 50$, and 100 as well as $AR = 1, 2$, and 4.

1. Reynolds number effect

For the accelerated motions, we first consider the Reynolds number effect on the aerodynamic forces for the $AR = 4$ flat plate accelerating from rest up to a freestream velocity corresponding to $Re = 14, 25, 50$, and 100 over one chord length of travel, as shown in Figure 8. At the beginning of the motion, there is a jump in both the lift and the drag forces due to the initial impulse of the acceleration profile. Thereafter, the coefficient of lift gradually increases for each of the Reynolds numbers considered. We observe that while the lift generated is similar for the $Re = 14, 25, 50$, and 100 cases, there are major differences in the drag resulting from this accelerated motion at such low Reynolds numbers.

Next, we consider the three-dimensional flowfield over the flat plate wing for the accelerated motion over one chord length of travel at $Re = 14, 25, 50$, and 100. Figure 9 shows the wake vortices visualized by iso-surfaces of $Q = 0.5$ for all Reynolds numbers considered. We start by visualizing the flowfield at $\tau = 0$ which corresponds to the beginning of the accelerated motion. Similar flow fields are observed during the

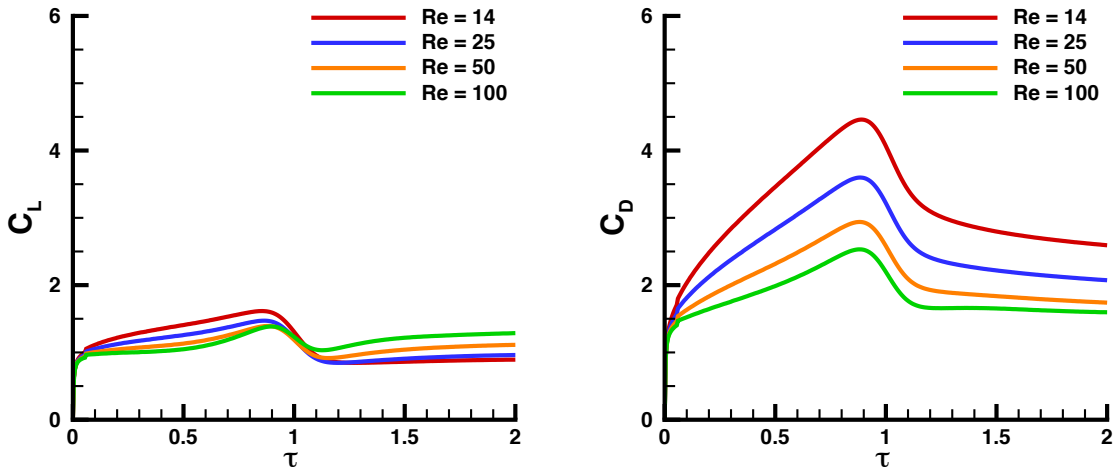

Figure 8. Reynolds number effect on the aerodynamic loading for $AR = 4$ wing accelerating over one chord length of travel.

accelerating phase of the motion. At $\tau = 1$, similar characteristics of the flowfield are observed with that of the pitching cases previously mentioned for $Re = 50$ and 100; counter-rotating tip vortices are generated due to the pressure difference at the top and bottom surfaces of the wing, the starting vortex has begun to roll up at the trailing-edge of the wing, and a leading-edge vortex has rolled up over the top surface of the wing and is attached to the corners of the leading edge. For the two lower Reynolds numbers considered, we observe no strong formation of the leading-edge, trailing-edge, and tip vortices. As the flat plate continues to translate, the leading-edge vortex for $Re = 50$ and 100 detaches from the wing and resembles the hairpin vortex previously observed for the pitching cases, whereas for the $Re = 14$ and 25 cases, the vortex structure remains smeared around the edges of the wing because of the dominant viscous diffusion of vorticity. At this low of Reynolds number, we are essentially observing Stokes flow over the wing.

2. Aspect ratio effect

We now consider the effect that the aspect ratio has on the aerodynamic forces for the flat-plate accelerating over one chord length of travel operating at $Re = 100$, given by Figure 10. The three aspect ratios considered for this study include $AR = 1, 2$ and 4. Initially, the lift and drag forces jump due to the impulsive start of the acceleration profile. As the plate accelerates from rest up to a constant freestream, there are little differences in the slope of the lift and drag curve for each aspect ratio considered. The only difference is the magnitude of the instantaneous lift and drag, where the higher the aspect ratio, the higher the force generated on the plate. After the accelerated motion has completed by $\tau = 1$, there is still an offset of the lift and drag forces for the three different aspect ratios.

Next, we consider the three-dimensional flowfield over the accelerating flat-plate wing of aspect ratios of $1, 2$, and 4, given in Figure 11. By the end of the accelerated motion, the counter-rotating tip vortices have rolled up due to the difference in pressure on the top and bottom surfaces of the wing, the starting vortex has begun to roll up at the trailing edge of the wing, and a leading-edge vortex has begun to roll up on the top surface of the wing. The three-dimensional vortex structure for the $AR = 1, 2$, and 4 wings appear to be similar early in time. As the plate continues to translate after the accelerated portion of the motion has completed, the leading edge vortex detaches from the corners of the leading edge for the $AR = 2$ and 4 wings, but stays stably attached for the $AR = 1$ wing due to the relatively large tip effects towards the centerline of the wing. We also notice that at later times, the hairpin vortex structure that evolves from the leading-edge vortex stays closer to the surface of the wing for the $AR = 2$ wing compared to the $AR = 4$, which is once again due to the tip effects that the lower aspect ratio wings experience. This result is similar to what was observed for the pitching wing discussed in the previous section.

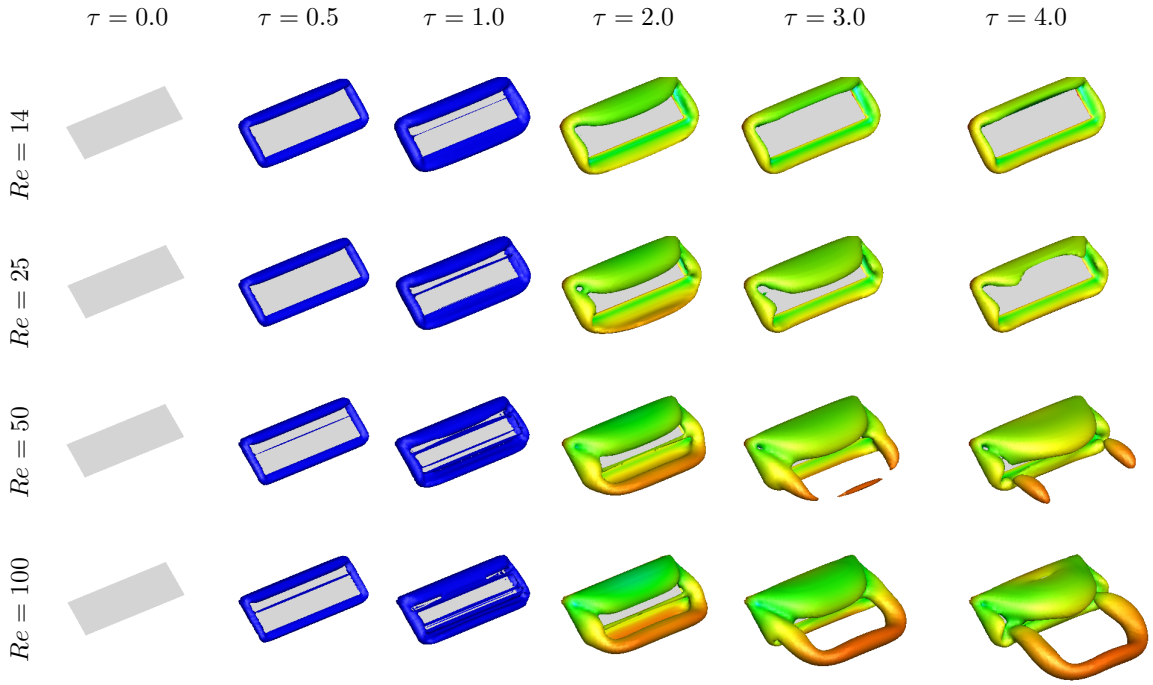

Figure 9. Flowfield images illustrating the Reynolds number effect for the $AR = 4$ wing accelerating over one chord length of travel. The Q-value used to visualize all Reynolds numbers considered is given by $Q = 0.5$, and is colored by contours of constant pressure.

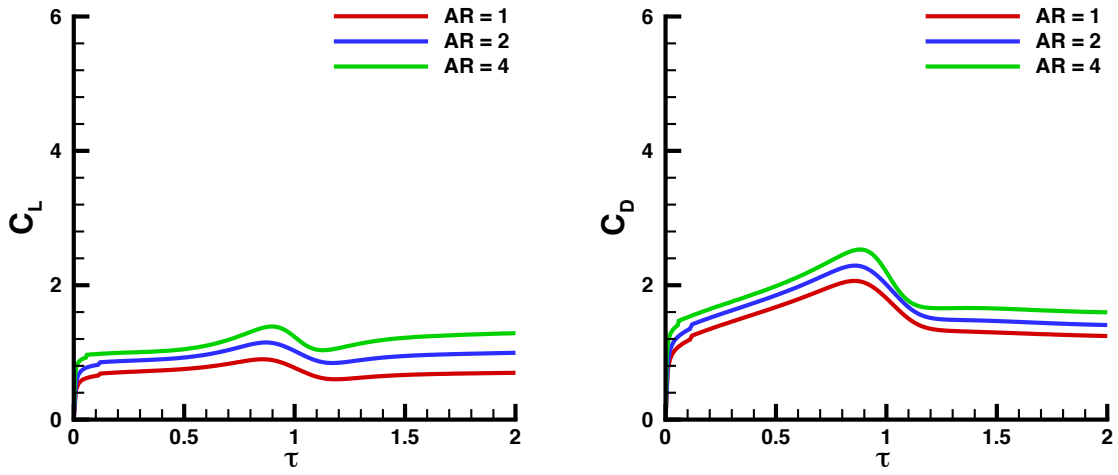

Figure 10. Aspect ratio effect on the aerodynamic loading for a wing accelerating over one chord length of travel at $Re = 100$.

IV. Conclusion

In the present study, we have investigated the influence of pitching and acceleration motions on the vortex dynamics around low-aspect-ratio wings. This included a parameter study of a range of low Reynolds numbers from $Re = 14$ to 500 and three different aspect ratios, $AR = 1, 2$, and 4. We have also compared the aerodynamic forces generated during these motions with that of water tunnel experiments performed at the Air Force Research Laboratory at a much higher Reynolds number of $Re = 10,000$. During the pitching motion over one chord length of travel (fast pitching), there is a good agreement between the force history

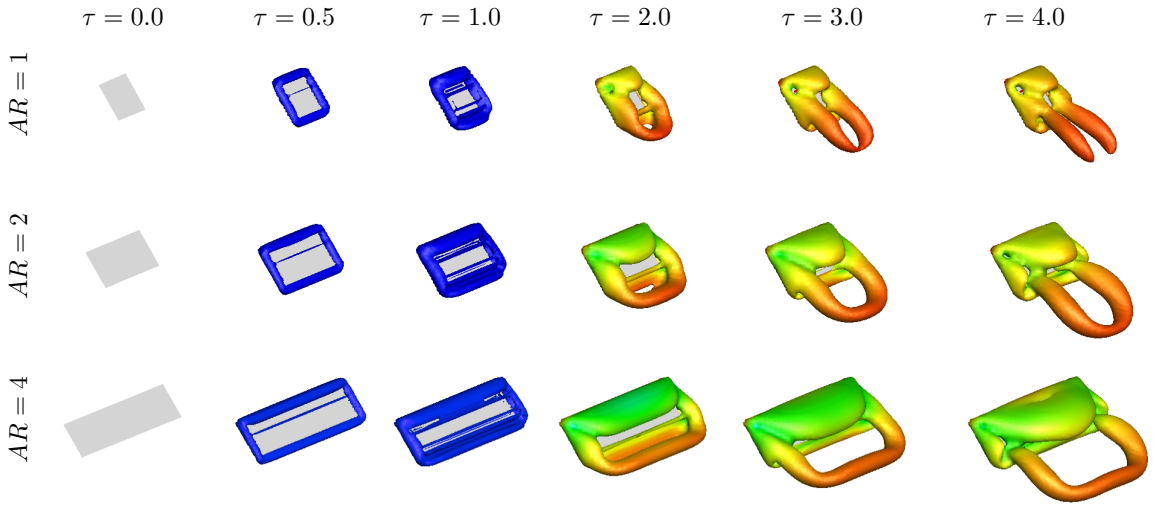

Figure 11. Flowfield images illustrating the effect of aspect ratio for a wing accelerating over one chord length of travel at $Re = 100$. The Q-value used to visualize all aspect ratios considered is given by $Q = 0.5$, and is colored by contours of constant pressure.

for the present simulations and the experimental data at much higher Reynolds number. As the Reynolds number is decreased for this pitching maneuver, there is an increase in the peak non-circulatory lift as well as a reduction in the slope of the lift curve. We observed that the vortex structure for the Reynolds numbers considered in this study had similar features with respect to the leading-edge, trailing-edge, and tip vortices, where the only main difference observed included the instabilities that began to creep into the flow for the higher Reynolds numbers. This was not the same case for the parameter study of the aspect ratio dependency on the aerodynamic forces and vortex structure. The aspect ratio has a much greater effect on the forces generated during the pitching motion and the vortex structure formed over the $AR = 1$ and 2 case differs from the $AR = 4$ case due to the increased tip effects effecting the centerline of the wing.

We also considered the forces and vortical structure generated during a linear accelerated motion, where the flat-plate wing accelerated from rest in a quiescent fluid up to a maximum velocity at a fixed angle of attack of $\alpha = 45°$. We have concluded from this study that a very low Reynolds numbers from $14 - 100$, the drag force on the flat-plate wing than the lift force. Although the vortex structure for the Reynolds numbers considered in the acceleration portion of this study have many similarities to that observed for the pitching wing at the corresponding Reynolds numbers, the pitching wing produces a much higher lift force for the one chord length of travel motions. These acceleration simulations will be studied further in collaboration with experiments at AFRL to gain insight on the aerodynamic forces generated during this maneuver at very low Reynolds numbers.

V. Acknowledgments

RJ and KT were supported by the USAF Air Vehicles Directorate Summer Research and Development Program during their stay at the Wright–Patterson Air Force Base.

References

[1]Taira, K. and Colonius, T., "Three-dimensional flows around low-aspect-ratio flat-plate wings at low Reynolds numbers," *J. Fluid Mech.*, Vol. 623, 2009, pp. 187–207.

[2]Granlund, K., Ol, M., and Bernal, L., "Experiments on pitching plates: Force and flowfield measurements at low Reynolds numbers," AIAA Paper 2011-872, 2011.

[3]Chen, K. K., Colonius, T., and Taira, K., "The leading-edge vortex and quasisteady vortex shedding on an accelerating plate," *Phys. Fluids*, Vol. 22, No. 3, 2010, pp. 033601.

[4]Garmann, D. J. and Visbal, M. R., "Numerical investigation of transitional flow over a rapidly pitching plate," *Phys. Fluids*, Vol. 23, No. 9, 2011.

[5]Yilmaz, T. O. and Rockwell, D., "Flow structure on finite-span wings due to pitch-up motion," *J. Fluid Mech.*, Vol. 691,

2012, pp. 518–545.

[6]Calderon, D. E., Wang, Z., Gursul, I., and Visbal, M. R., "Volumetric Measurements and Simulations of the Vortex Structures Generated by Low Aspect Ratio Plunging Wings," Vol. AIAA Paper 2009-0914, 2012.

[7]Lee, J.-J., Hsieh, C.-T., Chang, C. C., and Chu, C.-C., "Vorticity forces on an impulsively started finite plate," *J. Fluid Mech.*, Vol. 694, 2012, pp. 464–492.

[8]Granlund, K., OL, M. V., Taira, K., and Jantzen, R., "Parameter Studies on Rotational and Translational Accelerations of Flat Plates," AIAA Paper 2013-XXXX, 2013.

[9]Taira, K. and Colonius, T., "The immersed boundary method: a projection approach," *J. Comput. Phys.*, Vol. 225, 2007, pp. 2118–2137.

[10]Eldredge, J., Wang, C., and OL, M., "A computational study of a canonical pitch-up, pitch-down maneuver," AIAA Paper 2009-3687, 2009.

[11]Hunt, J., Wray, A., and Moin, P., "Eddies, Streams, and Convergence Zones in Turbulent Flows," Center for Turb. Research, Stanford Univ., 1988.

[12]Visbal, M., "Flow Structure and Unsteady Loading Over a Pitching and Perching Low-Aspect-Ratio Wing," AIAA Paper 2012-3279, 2012.